Surface & Coatings Technology 496 (2025) 131660

Contents lists available at ScienceDirect

Surface & Coatings Technology

journal homepage: www.elsevier.com/locate/surfcoat

Tribo-corrosion behavior of hypoeutectoid and hypereutectoid TC4-Cu coatings fabricated by laser surface alloying

Q. Qiao [a], V.A.M. Cristino [a], L.M. Tam [a,b], C.T. Kwok [a,c,*]

[a] Department of Electromechanical Engineering, University of Macau, Macao
[b] Institute for Development and Quality, Macao
[c] Institute of Applied Physics and Materials Engineering, University of Macau, Macao

ARTICLE INFO

Keywords:
TC4-Cu coatings, laser surface alloying
Tribo-corrosion
Synergism

ABSTRACT

In this study, tribo-corrosion behavior of TC4-Cu coatings with hypoeutectoid and hypereutectoid compositions (6 and 17 *wt*% Cu) on TC4 (Ti6Al4V) fabricated by laser surface alloying (LSA) was investigated. LSAed TC4-Cu coatings displayed a higher tribo-corrosion resistance than that of pristine TC4 in 0.9 *wt*% NaCl solution at 37 °C owing to lower friction coefficient (COF), higher hardness and nobler open circuit potential (*OCP*). Tribo-corrosion of the LSAed TC4-Cu coatings was found to be dominantly attributed to mechanical wear, followed by wear-induced corrosion, while the electrochemical corrosion was negligible. The tribo-corrosion resistance of the LSAed TC4-Cu coatings was significantly enhanced because of the existence of the hard intermetallic phases (Ti_2Cu and TiCu), which effectively inhibit plastic deformation, reduce removal loss and galvanic effect between the worn and unworn regions during the tribo-corrosion process. The Cu-bearing TC4 coatings developed in this study demonstrate excellent tribo-corrosion resistance with effective anti-bacterial properties, suggesting their promising applications in the biomedical field.

1. Introduction

Ti6Al4V titanium alloy (TC4) is extensively applied as the body implants in orthopedics and dentistry due to their high mechanical resistance, outstanding corrosion resistance and biocompatibility [1–4]. Nevertheless, it is necessary to surmount a number of challenges, one of which being the ineffective antibacterial agent when TC4 is used as the body implants [5]. On the other hand, another weakness of TC4 is its low tribological resistance leading to low durability [6]. Therefore, developing novel titanium alloys with improved performance is crucial. Copper (Cu), an element possesses strong antimicrobial properties that have been employed to generate the bulk TC4-Cu alloys, which could effectively inactivate different microbes by direct contact mechanism [7]. Hypoeutectoid TC4-Cu alloys with Cu content lower than 7.1 *wt*% with controlled grain structure and desirable properties are suitable for manufacturing rings, disks, and blades of jet engines [8]. While hypereutectoid TC4-Cu alloys with Cu content higher than 7.1 *wt*% are used for medical uses owing to their excellent anti-bacterial efficacy [8]. Zykova and co-workers reported that TC4-5*wt*%Cu alloy produced by electron-beam additive manufacturing possessed higher tensile strength (1126 MPa) than that of TC4 (906 MPa) due to the presence of intermetallic phase (IMP) Ti_2Cu [9]. Meanwhile, Peng et al. reported that the Ti6Al4V-*x*Cu alloys ($x = 4.5$, 6 and 7.5 *wt*%) fabricated by hot-processing exhibited higher yield strength (965 MPa) and tensile strength (1100 MPa) than those of TC4, owing to more Ti_2Cu [10]. On the other hand, the corrosion resistance of the sintered Ti—Cu alloy was found to be increased by the findings of Zhang and his-coworkers, who suggested that dissolution of the alloy could be inhibited by adding Cu [11]. In addition, it was reported that the TC4-5*wt*%Cu produced by ingot melting displayed a stronger antibacterial property with the greater antibacterial rate (98.6 %) against *Staphylococcus aureus* compared to TC4 (50 %) [12]. However, most of the published work are focused on the hypoeutectoid TC4-Cu alloys and the comparison of the tribo-corrosion between the hypoeutectoid and hypereutectoid TC4-Cu alloys is not reported in the literature.

In fact, one of the crucial requirements for the alloys for engineering and medical applications is desirable tribo-corrosion resistance. The degradation induced by the combined effect of mechanical wear and electrochemical corrosion, i.e. tribo-corrosion, is more serious than these two processes functioning separately [13,14]. During tribo-corrosion, the combination of high burdens of frictional contact and aggressive media for Ti-based alloy usually leads to a synergy and

* Corresponding author at: Department of Electromechanical Engineering, University of Macau, Macao.
E-mail address: fstctk@umac.mo (C.T. Kwok).

https://doi.org/10.1016/j.surfcoat.2024.131660
Received 13 October 2024; Received in revised form 28 November 2024; Accepted 9 December 2024
Available online 10 December 2024

enhanced material degradation [15,16]. Tribo-corrosion behavior of selectively laser-melted TC4 in simulated body fluid has been explored, the tribo-corrosion resistance was improved owing to the oxide layer formed on the surface [17]. While there is currently a dearth of work on the tribo-corrosion of the Cu-containing titanium alloys and coatings.

Laser surface alloying (LSA) is an efficient surfacing process which employs the high laser energy density to melt the coatings and a small part of the substrate beneath. Owing to fast quenching and high solidification rate during the LSA process, refined microstructure, homogenized compositions, extended solid solubility and improved surface properties could be achieved [18]. In the previous study of the present authors, the hardness of the LSAed TC4-Cu were found to be significantly enhanced owing to the existence of the hard intermetallic phases [18]. In the stagnant 0.9 *wt*% NaCl solution at 37 °C, the LSAed TC4-6wt %Cu showed the mild micro-galvanic effect between intermetallic phases (cathode) and α-Ti (anodes) whereas the LSAed TC4-17wt%Cu was less corrosion resistant because of the more severe micro-galvanic effect between the intermetallic phases and the α-Ti/β-Ti [18]. With the different Cu contents in the LSAed TC4-Cu coatings, the hypoeutectoid coating (6 wt% Cu) consists of a primary Ti-rich metallic phase and a secondary Cu-rich phase (Ti_2Cu). with higher ductility and toughness. While hypereutectoid coating (17 *wt*% Cu) has a more Cu-rich phase (Ti_2Cu) with increased hardness and strength. Hence, it is expected the hypoeuctectoid and hypereutectoid coatings possess different resistance against tribo-corrosion in 0.9 *wt*% NaCl solution. In the present work, the influence of Cu content on the tribo-corrosion behavior of the LSAed TC4-Cu coatings with hypoeutectoid and hypereutectoid compositions in 0.9 *wt*% NaCl solution at 37 °C is examined by means of the electrochemical measurement and the ball-on-plate tribometer. Moreover, the synergism between mechanical wear and electrochemical corrosion of the LSAed TC4-Cu coatings is explored to further analyze the tribo-corrosion mechanism.

2. Experimental methods

2.1. Specimen preparation

TC4 plates with size of 20 mm × 20 mm × 4 mm were utilized as the substrate for LSA and its compositions are depicted in Table 1. To increase the surface roughness of the plates for better adhering with the pure Cu powder, they were taken for mechanically grinding with the 80-grit sand paper. The pure Cu powder (average diameter: 75 μm) and the polyvinyl alcohol (PVA, 4 *wt*%) were mixed together as the slurry. Using a paintbrush, the slurry was painted on the plate surface and the thicknesses of the pure Cu layers (t) was controlled to be about 25 and 50 μm by weight method (Table 1). Then the TC4 plates pre-placed with pure Cu powder were dried with a fan heater and then LSAed using a high-power diode laser (HPDL, LDM 1000–1000, Laserline, Germany). The laser beam at power of 2 kW and diameter of 2 mm was delivered with an optical fiber, and the scanning speeds (v) of 20 and 40 mm/s were utilized for processing the LSAed specimens (Table 1). The basis for selecting the LSA parameters was to control the degree of dilution of Cu in the LSAed TiAlVCu coatings for achieving hypoeutectoid and hypereutectoid compositions. A thicker preplaced Cu layer allowed a higher Cu content to be alloyed in the alloyed zone. On the other hand, a higher laser scanning speed allowed a shorter interaction time between the laser beam and the pre-placed specimen leading to a lower degree of dilution and hence a higher Cu content. For the LSAed specimen TC4-6Cu with lower Cu content (6 wt%, hypoeutectoid composition), a thin pre-placed layer (25 μm) and a lower laser scanning speed (20 mm/s) were used, while for the specimen TC4-17Cu with higher Cu content (17 wt%, hypereutectoid composition), a thicker pre-placed layer (50 μm) and higher laser scanning speed (40 mm/s) were applied. Parallel tracks were successively overlapped on the surface by 50 % for fabricating the alloyed layers. To prevent the specimens from oxidation, an Argon gas shroud was utilized and the flow rate was set at 15 L/min. The LSAed TC4 with different Cu contents were fabricated by controlling t and v. The dilution ratio (DR) indicating the degree of dilution of Cu in the LSAed layer was determined by $DR = (1\text{-}t/D) \times 100$ %, where D is the depth of the alloyed layer. The detail of specimen preparation can be found in a previous work of the present authors [18]. After LSA, the compositions of the LSAed specimens were analyzed using energy dispersive X-ray spectroscopy (EDS, Horiba EX-250, Japan). The scanning-electron microscope (SEM, Hitachi S-3400 N, Japan) was used to observe the microstructure of the specimens and the X-ray diffractometer (XRD, Rigaku MiniFlex 600, Japan) was used to identify the phases present and was operated at 40 kV and 40 mA using Cu Kα radiation, and a scanning rate of 0.25°/s. The software 'ImageJ' was applied to acquire the volume fraction of the formed intermetallic phases in the LSAed specimens.

2.2. Corrosion test under quiescent condition

Prior to the electrochemical measurements, the LSAed specimens and pristine TC4 (i.e. the working electrodes) were polished with 1-μm diamond paste to achieve an average surface roughness (R_a) of 0.05 μm conforming to ASTM Standard G133-22 [19]. A three-electrode electrochemical cell containing 0.9 *wt*% NaCl solution was used for measuring the potential and current through potentiostat (PAR Versastat 3F, Princeton, USA). The solution temperature was monitored at 37 ± 1 °C with an electronic thermostat. The exposed area of the specimen to the solution was about 1 cm^2. A standard Ag/AgCl electrode (+0.197 V vs. SHE at 25 °C) was utilized as the reference electrode (RE) while a platinum sheet was acted as the counter electrode (CE). For each specimen, the open circuit potential (*OCP*) was stabilized after 3600 s, and then potentiodynamic polarization (PD) test was conducted in the potential range of −0.25 to +1.2 V (vs. Ag/AgCl) with the scanning rate of 1 mV/s. The corrosion potential (E_{corr}) and corrosion current density (I_{corr}) were obtained from the PD curves using Tafel extrapolation method with the software 'PowerCorr'.

2.3. Tribo-corrosion test

To simulate the environment of the human body, all tribo-corrosion tests were performed using a ball-on-plate tribometer (UMT-2, Bruker, USA) connected to an electrochemical workstation (Fig. 1) in 0.9 *wt*% NaCl solution at 37 °C in accordance with ASTM Standard G119-09 [20]. The electrochemical cell was filled with 50 mL of freshly prepared 0.9 *wt* % NaCl solution for the tribo-corrosion test. The temperature of the solution was maintained at 37 °C by the electronic thermostat. The Al_2O_3 ball with diameter of 5 mm was slid against the specimen in reciprocating mode under a normal load of 20 N, with a frequency of 0.1

Table 1
LSA parameters[a] and compositions of pristine TC4 and LSAed TC4-Cu.

Sample	t (μm)	v (mm/s)	D (mm)	DR (%)	Compositions (*wt.%*)			
					Ti	Al	V	Cu
TC4	–	–	–	–	90.3 ± 3.3	6.1 ± 0.1	3.6 ± 0.3	–
TC4-6Cu	25	20	1.02 ± 0.07	97.7	85.3 ± 2.5	5.9 ± 0.1	2.8 ± 0.4	6.0 ± 0.1
TC4-17Cu	50	40	0.79 ± 0.06	93.6	74.3 ± 2.6	5.4 ± 0.1	3.2 ± 0.1	17.1 ± 0.7

[a] t is the thickness of pre-placed Cu layer, v is the laser scanning speed, D is the depth of the alloyed zone and DR is the dilution ratio.

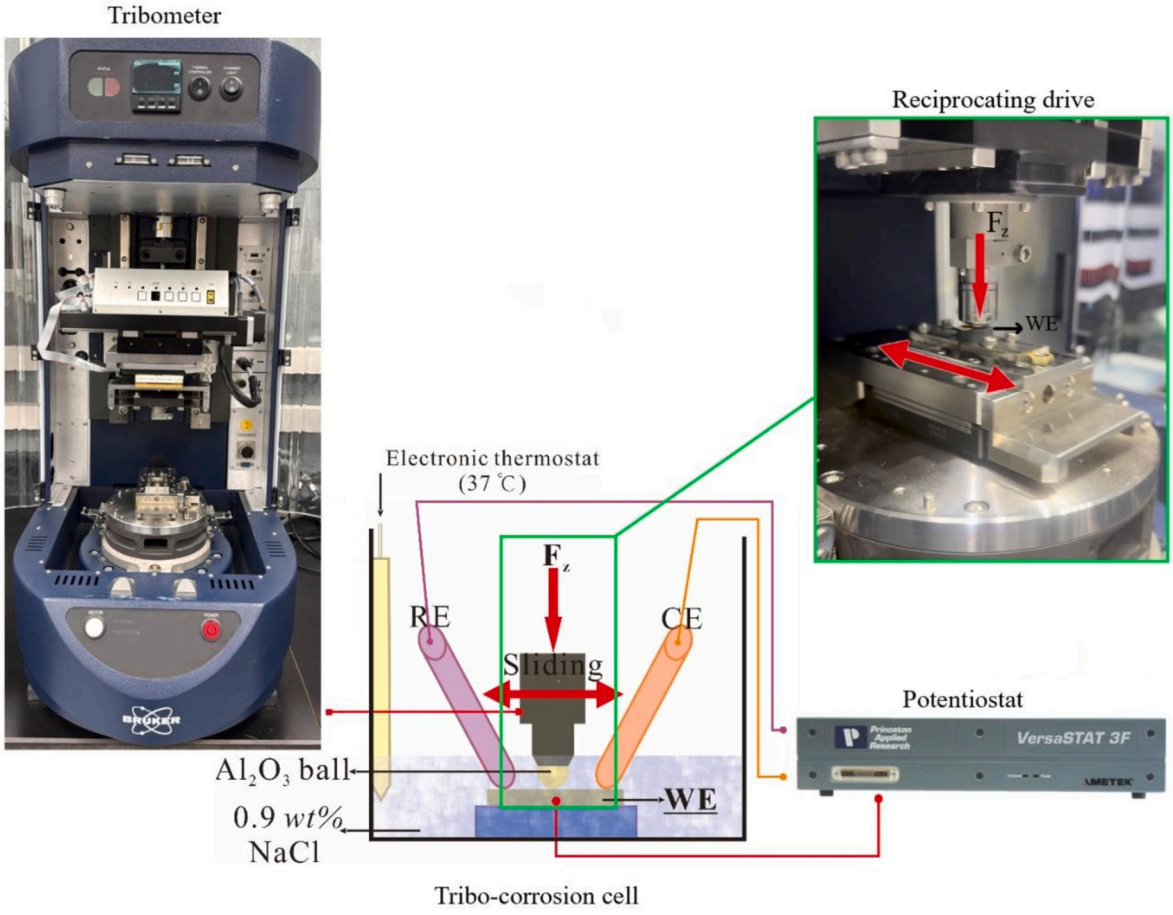

Fig. 1. Setup for tribo-corrosion test.

Hz and a stroke length of 3 mm. Before sliding, the specimens were immersed in the solution for an hour to reached equilibrium. *OCP* was monitored for 300 s before sliding, then the Al_2O_3 ball was slid against the specimens for 1800 s and both *OCP* and coefficient of friction (COF) were recorded simultaneously. Finally, the *OCP* was measured for further 300 s without load. Polarization under tribo-corrosion condition was also performed to analyze the effect of mechanical wear on corrosion, sweeping the potential range from −0.25 to 1.2 V (vs. Ag/AgCl) at a scanning rate of 1 mV/s. It was then assessed over a sliding distance of 18 m for 1800 s. The I_{corr} and E_{corr} were also extracted under tribological condition. Moreover, the tribo-corrosion test was also conducted in cathodic condition at the potential −1 V (vs. Ag/AgCl) for 1800 s. Under such condition, the wear loss was obtained due to the pure mechanical wear (without electrochemical effect) [21,22]. After the tribo-corrosion test, the morphologies of the worn surface of the specimens were observed using the 3D optical microscope (Contour GT-X3, Bruker, USA) which was equipped with a software (VISION64, Bruker, USA) for measuring the volume loss. The surface profiles across the wear track were measured and its volume loss was estimated by multiplying the area of the profiles at heights below zero (with reference to the unworn region) with the length of the wear track [23]. All the tests were performed in triplicate for reproducibility.

2.4. Calculation of tribo-corrosion synergism

The synergism of electrochemical corrosion and mechanical wear was performed conforming to ASTM Standard G119-09 [20]. The total material loss rate, T (mm/yr) is the sum of all components (i.e. pure mechanical wear rate W_0, electrochemical corrosion rate C_0 and their synergism S), S was obtained from the interaction of electrochemical corrosion and mechanical wear, by the following equation [20]:

$$T = W_0 + C_0 + S \tag{1}$$

where T and W_0 can be calculated by

$$T\frac{\Delta V}{A\Delta t} \times 24\left(\frac{h}{d}\right) \times 365\left(\frac{d}{yr}\right) \tag{2}$$

$$W_0\frac{\Delta V}{A\Delta t} \times 24\left(\frac{h}{d}\right) \times 365\left(\frac{d}{yr}\right) \tag{3}$$

where ΔV is the volume loss (mm^3) of the specimen exposed for Δt (h), and A is the exposed area of the specimen (1 cm^2). T (in the corrosive medium) and W_0 (in air) are determined using Eqs. (2) and (3) respectively.

C_0 (mm/yr) is the electrochemical corrosion rate under the quiescent condition. After the PD tests performed at a scan rate of 1 mV/s, C_0 was calculated from the I_{corr} ($\mu A \cdot cm^{-2}$) conforming to ASTM Standard G102-89 [24]:

$$C_0 = K\frac{I_{corr}}{\rho}EW \tag{4}$$

where

$$\frac{1}{\rho} = \frac{W_{Ti}}{\rho_{Ti}} + \frac{W_{Al}}{\rho_{Al}} + \frac{W_V}{\rho_V} + \frac{W_{Cu}}{\rho_{Cu}} \tag{5}$$

$$EW = \left(\sum \frac{n_i w_i}{A_i}\right)^{-1} \tag{6}$$

and K is a constant (3.27×10^{-3} mm·g/(μA·cm·yr)), ρ represents the densities of the metallic elements ($\rho_{Ti} = 4.51$ g/cm^3, $\rho_{Al} = 2.70$ g/cm^3, $\rho_V = 6.00$ g/cm^3, and $\rho_{Cu} = 8.94$ g/cm^3), which can be calculated using the weight fractions of Ti, Al, V and Cu (see Table 1) with the rule of mixture, i.e., Eq. (5). The weight fractions of Ti, Al, V, Cu in the LSAed specimens is the W_{Ti}, W_{Al}, W_V and W_{Cu}, respectively ($W_{Ti} + W_{Al} + W_V + W_{Cu} = 1$). The equivalent weight (EW) is defined in Eq. (6) where W_i is the weight fraction, n_i is the valence and A_i represents the atomic mass of the ith element in the specimens.

S represents the material loss rate resulting from the synergism between electrochemical corrosion and mechanical wear of the specimens, including the corrosion induced wear (ΔC_W) and the wear induced corrosion (ΔW_C). Hence,

$$S = \Delta C_w + \Delta W_C \tag{7}$$

$$C_W = \Delta C_w + C_0 \tag{8}$$

$$W_C = \Delta W_C + W_0 \tag{9}$$

where C_W is the total corrosion component of T and can be measured by electrochemical means by Eq. (4), I_{corr} is extracted from the potentiodynamic polarization curve under sliding. W_C is the total wear component of T, which can be calculated through Eqs. (7)–(9).

3. Results and discussion

3.1. Microstructure

The cross-sections of the alloyed layers of the LSAed specimens TC4-6Cu (6 wt% Cu, hypoeutectoid composition) and TC4-17Cu (17 *wt*% Cu, hypereutectoid composition) are shown in Fig. 2a and b respectively. No defects are detected in the alloyed layers and a strong metallurgical bond is formed between the TC4 substrate and the alloyed layers. From Fig. 2(a-b) and Table 1, the average thicknesses of the alloyed zones (D) were calculated from 5 different locations of the LSAed coatings (Table 1). The alloyed layer of TC4-17Cu (about 0.79 ± 0.06 mm) is thinner than that of TC4-6Cu (about 1.02 ± 0.07 mm), which is attributed to the higher scanning speed. It means that the interaction time between the laser beam and substrate is shorter resulting in a faster cooling rate and forming a thinner alloyed layer [25]. The microstructures of the LSAed specimens are displayed in Fig. 2c-d. The interdendritic phase (the brighter zone c-2 as shown in Fig. 2c) is observed in TC4-6Cu. It is confirmed to be the intermetallic phase (Ti_2Cu) based on the atomic ratio of Ti (64.1 *at*.%) and Cu (28.5 *at*.%), i.e. 2:1 as shown in Table 2. Through the eutectoid reaction, the Ti_2Cu formed at the boundaries of α-Ti of LSAed specimens with brighter contrast. The existence of the phases is identified from the corresponding XRD patterns of the LSAed specimens (Fig. 2e) [26]. The standard JCPDS cards include No. 089-2762 (α-Ti), 044-1288 (β-Ti), 15-0717 (Ti_2Cu) and 07-0114 (TiCu) [27,28]. Using image analyzing, the volume fraction of Ti_2Cu in TC4-6Cu is found to be about 10.6 vol%. In addition to Ti_2Cu (the brighter zone d-2, Table 2), another intermetallic phase (TiCu) is detected in the LSAed specimen TC4-17Cu as the Cu content increase to 17.0 *wt*% after LSA (Fig. 2d). The atomic ratio of Ti (50.5 *at*.%) to Cu (45.6 *at*.%) is close to 1:1 (brighter zone, d-3, Table 2), and the existence of TiCu in TC4-17Cu is evidenced by the TiCu peaks in the XRD pattern (Fig. 2e) [18]. Besides, the β-Ti peak is observed in TC4-6Cu and TC4-17Cu. It is because in the process of α-Ti nucleation and the generation of other intermetallic phases, the ratio of β-Ti, Ti_2Cu and TiCu reach a dynamic metastable equilibrium, and the β-Ti could not be completely transformed into the new phase but was partially retained [29]. Meanwhile, the volume fraction of the intermetallic phases (Ti_2Cu and TiCu) in TC4-17Cu is approximately 35.9 vol%, which is higher than that in TC4-17Cu (10.6 vol%).

3.2. COF under OCP measurements

Fig. 3a displays the plots of coefficient of friction (COF) vs time of the specimens in 0.9 *wt*% NaCl solution at 37 °C and the average COF values are shown Table 3. The plot of COF vs time of the pristine TC4 exhibits fluctuation while the plots of the LSAed specimens are steadier. The ranking of the average COF in descending order is:

$$\text{TC4}\ (0.355 \pm 0.018) > \text{TC4}-6\text{Cu}\ (0.304 \pm 0.028) > \text{TC4}-17\text{Cu}\ (0.274 \pm 0.015)$$

It reveals that addition of Cu can decrease the COF of the LSAed TC4-Cu specimens. Dong et al. reported that decrease in average COF of the spark plasma sintered bulk Ti—Cu alloys was due to existence of Ti_2Cu [30]. On the other hand, the increase in hardness of the LSAed specimens with Cu leads to reduction in COF. It is more difficult for the counter surface (Al_2O_3) to press into the hard surfaces of TC4-6Cu (551 ± 21 $HV_{0.2}$) and TC4-17Cu (646 ± $HV_{0.2}$) [18]. With the decrease in contact area, the reduced frictional force consequently led to a lower COF for TC4-6Cu and TC4-17Cu [31]. Besides the effect of hardness, the induced passive film during corrosion also contributes to the lower COF. Liu and coworkers reported that the passive film of the Ti—Cu alloy fabricated by laser powder bed fusion (LPBF) contained TiO_2 and CuO detected using XPS [32]. Whereas only TiO_2 existed in the passive film of TC4 [32]. In addition, it was proved that the passive film on the surface of Ti—Cu alloy produced by LPBF was denser and thicker (12.04 nm) than that on the pure Ti (10.36 nm) [32]. Hence, it can be deduced that more stable passive films (TiO_2 and CuO) on TC4-Cu coatings result in redcued COF values (Fig. 3a and Table 3).

Fig. 3b displays the evolution of *OCP* for the specimens in 0.9 *wt*% NaCl solution at 37 °C before, during and after the sliding test. The *OCP* of the LSAed specimens were stable before sliding (from 0 to 300 s), indicating a stable oxide film was formed. It is observed that the *OCP* of TC4-6Cu is the noblest as compared with the pristine TC4 and TC4-17Cu under quiescent condition. The most active *OCP* of TC4-17Cu under the quiescent condition is attributed to the more severe micro-galvanic corrosion between the α/β-Ti and intermetallic phases (Ti_2Cu and TiCu) as reported by the previous work [18].

During sliding (from 300 to 2100 s), the *OCP* of all specimens shift remarkably in the active direction, indicating that the corrosion process was accelerated [33]. The natural passive film on the specimens was removed or disrupted from the surface because of the sliding action against the Al_2O_3 ball [34]. Yamamoto et al. reported that the passive layer on the surface of 312L stainless steel was destroyed during sliding in acidic solution and the freshly worn surface became more susceptible to corrosive-wear leading to a sharp active shift in *OCP* [35]. In the present study, the *OCP* keeps relatively stable with the elapsed time during sliding (Fig. 3b) because of the dynamic equilibrium between formation (re-passivation) and mechanical wear of the passive film [36,37]. From Table 4, the *OCP* of the pristine TC4, TC4-6Cu and TC4-17Cu under sliding ($OCP_{sliding}$) are actively shifted to −677.5 ± 30.8, −513.3 ± 18.2 and −478.7 ± 27.5 mV respectively, demonstrating increase in corrosion tendency.

When sliding terminated at 2100 s, the *OCP* gradually shifts to the nobler direction (Fig. 3b) because the damaged passive film was repaired when the axial force was removed [38]. It is also known as re-passivation of the active surface. The re-passivation rate shows the relevant characteristic of the tribo-corrosion of the metallic materials: faster the recovery of the surface, higher tribo-corrosion resistance [39]. From the zoomed inset graphs at the marked region (Fig. 3b), the LSAed specimens show a shorter re-passivation time, i.e., higher re-passivation rate [40,41]. The re-passivation rate is higher with the higher Cu content. But the final potentials (OCP_{final}) of all the specimens are lower than that before sliding ($OCP_{initial}$, Table 3), which means that the passive film cannot be completely restored in 300 s. The worn track caused by the tribo-corrosion during sliding stage (300–2100 s) still exists and

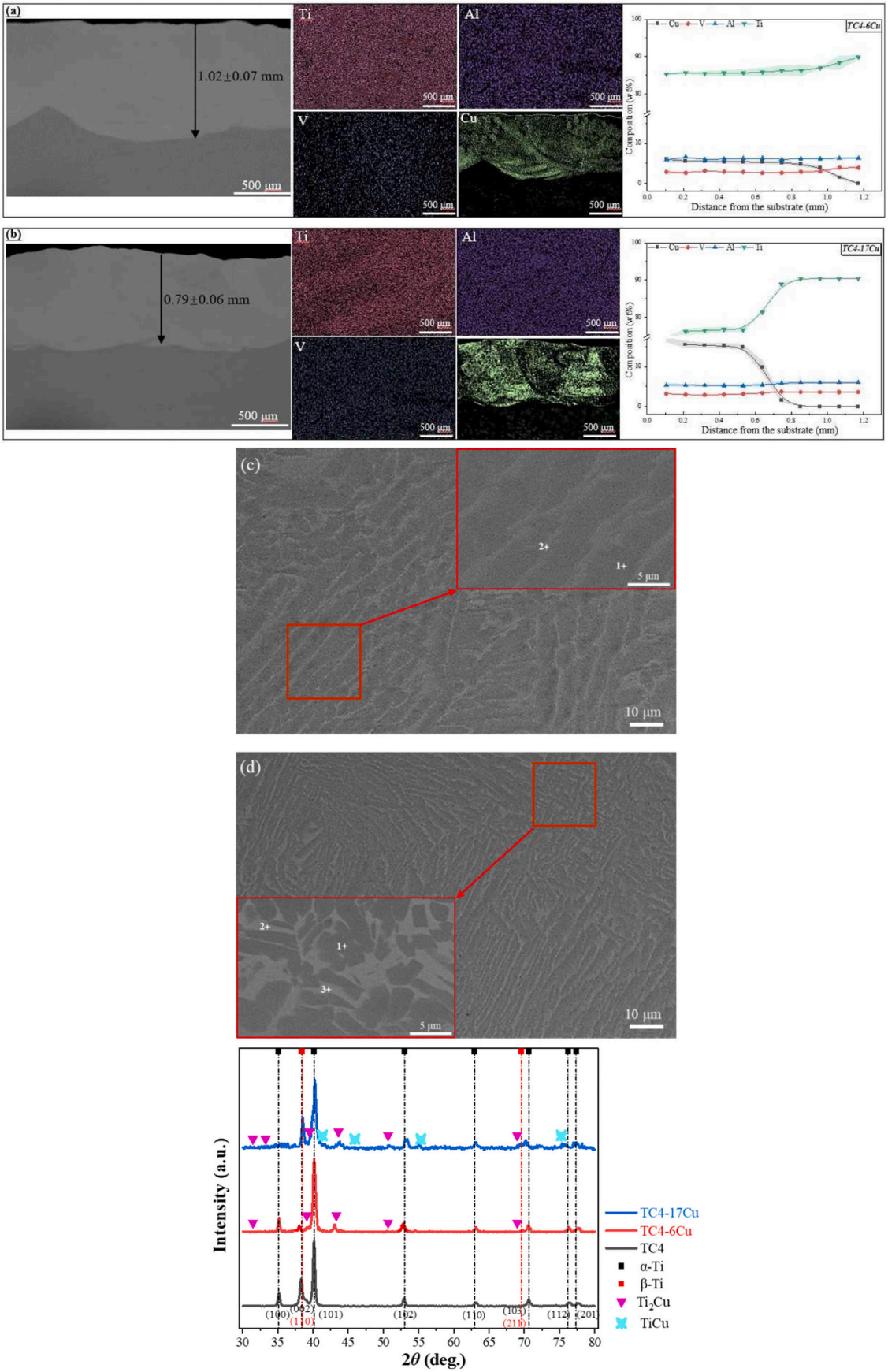

Fig. 2. Cross-section, EDS maps and compositional profiles of (a) TC4-6Cu and (b) TC4-17Cu; and microstructure of (c) TC4-6Cu and (d) TC4-17Cu, (e) XRD patterns of pristine TC4 and LSAed specimens.

Table 2
Compositions at different zones of LSAed specimens show in Fig. 2(c-d).

Zone	(wt%)				(at%)				Phase
	Ti	Al	V	Cu	Ti	Al	V	Cu	
c-1	92.7	3.3	2.3	1.8	90.9	5.7	2.1	1.3	α-Ti
c-2	60.0	3.2	1.4	35.4	64.1	6	1.4	28.5	Ti_2Cu
d-1	92.3	2.7	2.3	2.7	91.1	4.8	2.1	2.0	α-Ti
d-2	56.5	2.3	2.4	38.9	61.4	4.4	2.4	31.8	Ti_2Cu
d-3	44.2	1.0	1.7	53.0	50.5	2.1	1.8	45.6	TiCu

could be exposed to the solution leading to lower potential [42].

3.3. Potentiodynamic polarization

The polarization curves of the pristine TC4 and the LSAed specimens in 0.9 *wt*% NaCl solution at 37 °C under quiescent and sliding conditions are shown in Fig. 4. The corrosion parameters extracted from the curves are shown in Table 5. Sliding causes a remarkable influence on the corrosion behavior. Firstly, the curves under sliding condition are noisier than those under quiescent condition (Fig. 4b) as the contact surface between the test specimen and the Al_2O_3 ball could not be kept

Table 3
Average coefficients of friction (COF) during sliding in 0.9 *wt*% NaCl solution at 37 °C and hardness of various specimens.

Specimens	COF	Hardness ($HV_{0.2}$) [18]
TC4	0.355 ± 0.018	353 ± 6.5
TC4-6Cu	0.304 ± 0.028	551 ± 21
TC4-17Cu	0.274 ± 0.015	646 ± 18

Table 4
Average *OCP* before sliding ($OCP_{initial}$), during sliding ($OCP_{sliding}$) and after sliding (OCP_{final}) of various specimens against Al_2O_3 ball in 0.9 *wt*% NaCl solution at 37 °C.

Sample	$OCP_{initial}$ (mV)	$OCP_{sliding}$ (mV)	OCP_{final} (mV)
TC4	−374.7 ± 9.6	−677.5 ± 30.8	−405.2 ± 19.7
TC4-6Cu	−305.3 ± 10.8	−513.3 ± 18.2	−418.5 ± 16.7
TC4-17Cu	−399.4 ± 15.0	−478.7 ± 27.5	−433.6 ± 17.3

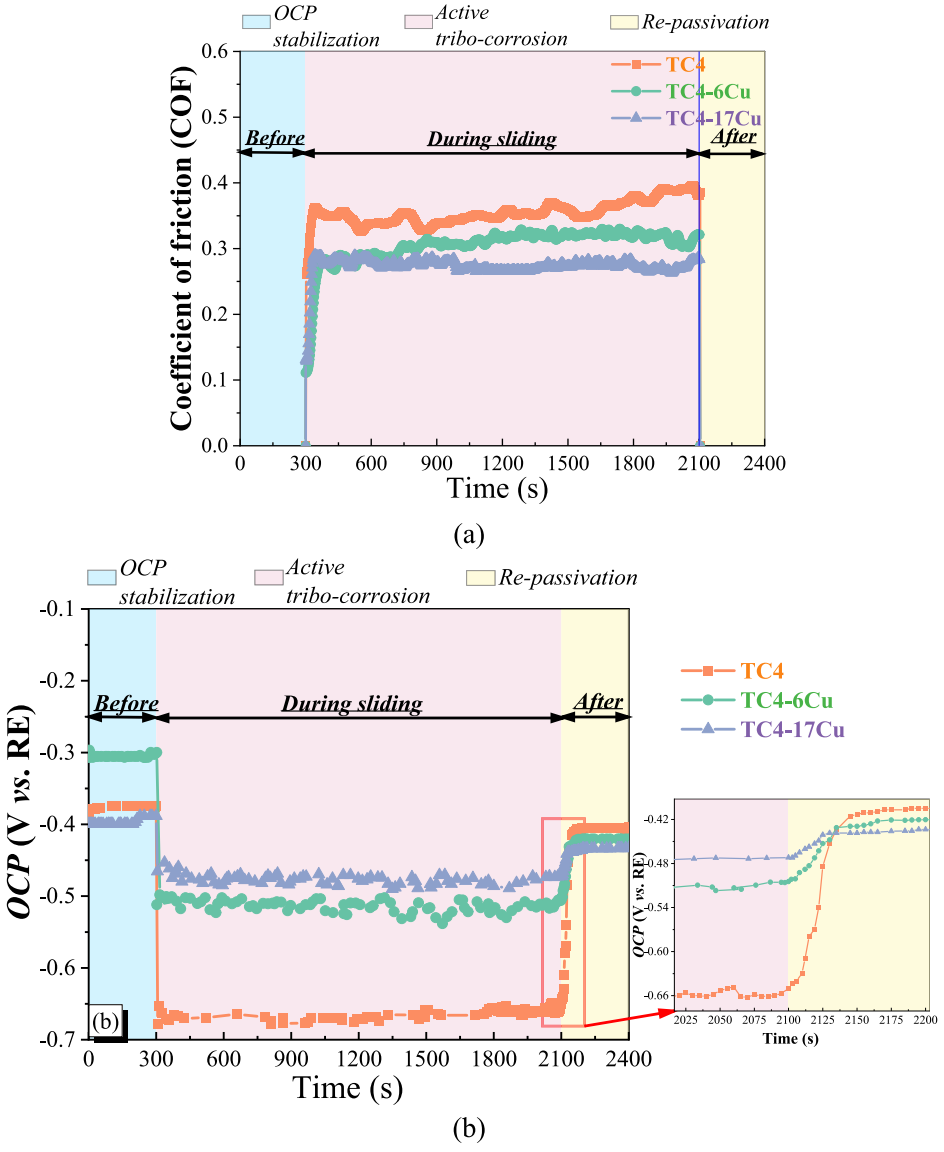

Fig. 3. (a) Plots of COF and (b) *OCP* vs. elapsed time of TC4 and LSAed specimens slid against Al_2O_3 balls in 0.9 *wt*% NaCl solution at 37 °C.

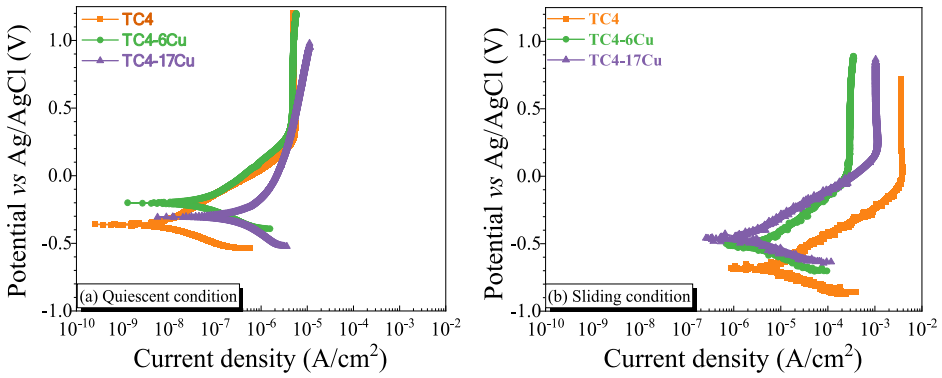

Fig. 4. Polarization curves of pristine TC4 and the LSAed specimens in 0.9 *wt*% NaCl solution at 37 °C under (a) quiescent and (b) sliding conditions.

Table 5
Corrosion parameters of TC4 and LSAed specimens.

Specimens	E_{corr} (mV)		I_{corr} (μA/cm^2)	
	Quiescent	Sliding	Quiescent	Sliding
TC4	−363.8 ± 18.5	−678.7 ± 31.1	0.057 ± 0.013	6.9 ± 0.4
TC4-6Cu	−197.8 ± 23.3	−504.4 ± 20.6	0.074 ± 0.010	5.0 ± 0.2
TC4-17Cu	−296.3 ± 28.5	−456.8 ± 24.1	0.480 ± 0.092	2.5 ± 0.2

constant during the tribo-corrosion process [43]. Compared to the results under the quiescent condition, the corrosion potential (E_{corr}) exhibits a significant shift in active direction and the corrosion current density (I_{corr}) significantly increases (Table 5). It is noticed that the I_{corr} under sliding condition are about 59.0–121.1 times those of the quiescent condition, demonstrating that the corrosion rate of the LSAed TC4-Cu specimens increase under sliding.

Under quiescent condition, it can be found that the corrosion resistance of the LSAed TC4-Cu reduces with the increase in the Cu content (Fig. 4a and Table 5). It can be observed that TC4-17Cu displays the lowest corrosion resistance under quiescent condition as the I_{corr} is about 8.4 times higher than that of pristine TC4. The larger volume fraction of the nobler intermetallic phases ($CuTi_2$ and CuTi, about 35.9 vol%) in TC4-17Cu results in a more significant micro-galvanic effect between the intermetallic phases (cathode) and α-Ti/β-Ti (anode) and in turn a higher corrosion rate [18].

On the contrary, adding Cu shows the opposite effect on the corrosion behavior of the LSAed TC4-Cu under sliding (Fig. 4b). Bao et al. [44] indicated that the Ti-3*wt*%Cu showed the lower I_{corr} (3.12 μA/cm^2) than that of cp-Ti (5.86 μA/cm^2) during sliding. Compared with the pristine TC4 and TC4-6Cu, the LSAed specimen with higher Cu content (i.e. TC4-17Cu) shows the highest corrosion resistance, with the noblest E_{corr} (−456.8 mV) and the lowest I_{corr} (2.5 μA/cm^2) under sliding condition (Table 5). It means that the influence of the micro-galvanic effect between the intermetallic phases and α/β-Ti on the tribo-corrosion behavior of the LSAed specimens is less significant in sliding condition as the phases are in active state during sliding.

3.4. Wear loss and worn surface morphology

Fig. 5 presents the 3D images of worn surfaces of the specimens after the sliding test in 0.9 *wt*% NaCl solution and the wear depth profiles along the line XY (across the worn track). From Table 6, the pristine TC4 shows the most seriously worn track with the largest wear volume (0.0051 mm^3). Whereas, it is observed that the LSAed specimens present the smaller volume loss. TC4-17Cu displays the highest tribo-corrosion resistance, with the smallest wear volume (0.0029 mm^3) (Table 6).

Fig. 6 shows the SEM micrographs of the worn surface of the specimens for further investigating their tribo-corrosion mechanism. The worn surface of the pristine TC4 was plastically deformed seriously with deepest abrasive groove due to its lower hardness, which typically shows adhesive and abrasive wear (Fig. 6a). In addition, compact oxide is present on the worn surfaces of all specimens owing to repetitive material transfer between the counter surfaces. The plastic deformation and grooves observed on the surface of the pristine TC4 exposed a larger effective surface area to the NaCl solution, leading to accelerated corrosion during the tribo-corrosion process [45,46]. Moreover, protection of the passive film on the pristine TC4 is destroyed when wear and corrosion occur simultaneously. From the EDS results (Fig. 6(a-II)), B and C sites contain much higher O content (up to 24.4 *wt*%), indicating the existence of titanium oxide on the worn surface of the pristine TC4. It is in line with the findings of Lu et al. [47], who found that some oxidized debris were produced during the sliding action between the TC4 and the counter surface. The oxidized debris kept sliding and then adhered to the surface, showing the occurrence of adhesive and abrasive wear.

As the passive film was removed, a new potential difference was created between the underlying fresh surface and the unworn surface and enhanced the corrosion and wear of the pristine TC4 [48]. For the LSAed specimens, the worn tracks are smoother and the grooves are shallower as the Cu content increases. For TC4-17Cu (Fig. 6c), the plough groove on the worn track is much alleviated. Also, plastic deformation is lessened considerably for the LSAed specimens which are harder than TC4 and more difficult to deform during the tribo-corrosion process [49]. The hardest TC4-17Cu possesses the highest resistance against the plastic deformation and a small area of peeling pits and some grooves are observed. EDS results also indicate that the worn debris formed on the LSAed specimens consists of lower oxygen content (Fig. 6 (c-II)) as compared to the pristine TC4. The oxygen content of TC4-6Cu and TC4-17Cu are in the range of 7.8 to 20.7 *wt*%. It means that the adhesion wear was obviously observed and TC4-17Cu possesses the highest tribo-corrosion resistance, which is supported by the hardness, and COF as well the lower I_{corr} during sliding condition (Figs. 3 and 4).

3.5. Synergism in tribo-corrosion

The synergism between electrochemical corrosion and mechanical wear is the dominant part for damaging the material during sliding against the Al_2O_3 ball in aggressive media [50]. Therefore, it is important to quantify the synergistic effect so as to further understand the tribo-corrosion mechanism. Based on Eqs. (1)–(9), the related parameters of the pristine TC4 and LSAed specimens are given in Table 7 and the contributions of tribo-corrosion components of various specimens are depicted in Fig. 7. The percentages W_0/T of the pristine TC4, TC4-6Cu and TC4-17Cu are 55.06 %, 53.39 % and 52.99 % respectively, indicating that the pure mechanical wear is the dominant component for the material removal of all specimens. On the other hand, the percentages contributed by corrosion (C_0/T) of the specimens are very small and it has very little influence on tribo-corrosion. The percentages of

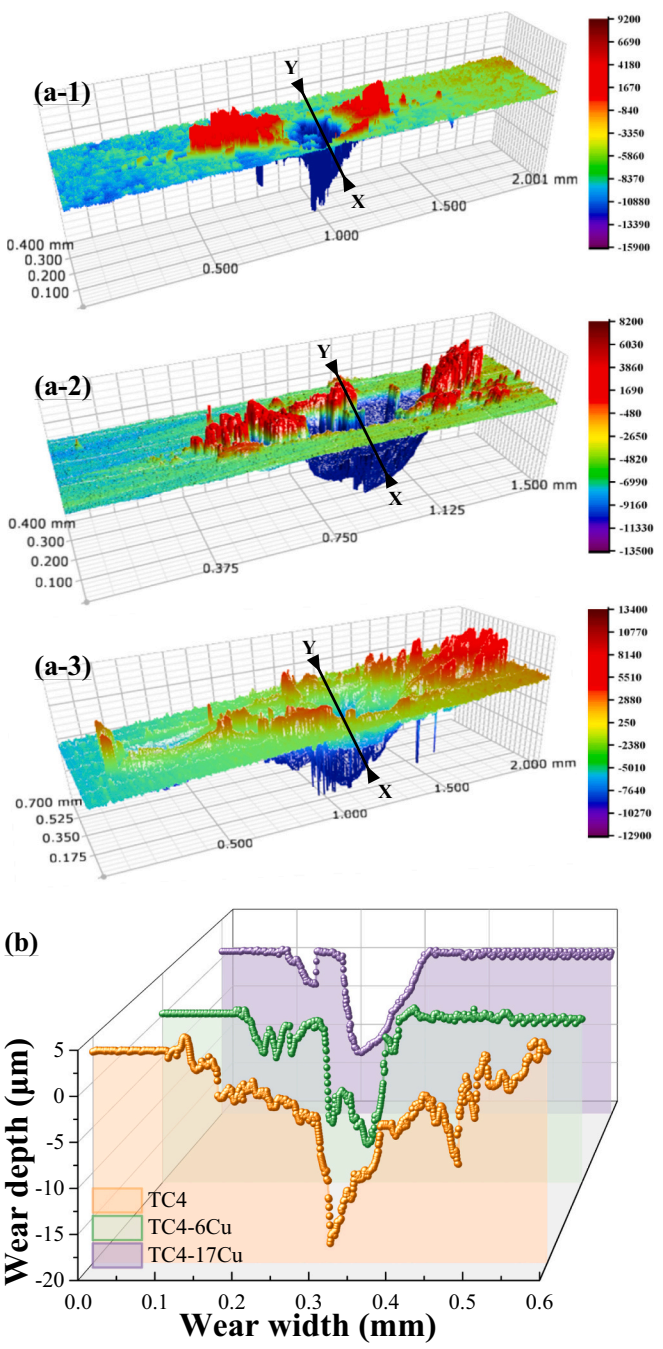

Fig. 5. (a) 3D images of worn surface of TC4 and LSAed specimens, and (b) 2D cross-sectional profiles of their worn surface along the lines XY in (a).

Table 6
Wear width, wear depth and wear volume of TC4 and LSAed specimens after tribo-corrosion test in 0.9 *wt*% NaCl solution at 37 °C.

Specimens	Wear width (mm)	Wear depth ($\times 10^{-5}$ mm)	Wear volume ($\times 10^{-2}$ mm^3)
TC4	0.392 ± 0.020	1.79 ± 0.12	0.51 ± 0.04
TC4-6Cu	0.374 ± 0.015	1.55 ± 0.08	0.39 ± 0.03
TC4-17Cu	0.199 ± 0.010	1.22 ± 0.06	0.29 ± 0.02

corrosion-induced wear ($\triangle C_W/T$) of the pristine TC4, TC4-6Cu and TC4-17Cu are 0.07 %, 0.06 % and 0.01 %, respectively. It is in accordance with the polarization results under sliding that the I_{corr} decreases as the Cu content increases (Table 5). Hence, it can be deduced that the pure mechanical wear is the domain factor leads to the material removal of the specimens. For TC4-17Cu, the contribution of mechanical wear (52.99 %) to removal loss is higher than those of electrochemical corrosion (3.60 %) and synergy (43.41 %).

At the same time, the wear and corrosion mechanisms of the LSAed specimens in 0.9 *wt*% NaCl solution under sliding is presented as the synergistic ratio of ΔC_W and ΔWc (a) as shown in Eq. (10).

$$a = \frac{\Delta C_w}{\Delta W_C} \tag{10}$$

When $a \leq 0.1$, mechanical wear is predominant during the process. The wear-induced corrosion is induced when the $0.1 < a \leq 1$. Corrosion is dominant in the tribo-corrosion systems when $1 < a \leq 10$ and the predominating process for material degradation is corrosion when the $a \geq 10$ [51]. From Table 7, the values of a of the pristine TC4, TC4-6Cu and TC4-17Cu are 0.00158, 0.00135 and 0.00021 respectively. It further confirms that the mechanical wear for the LSAed specimens is the main factor during the tribo-corrosion process. The removal loss of the specimens could be explained by the corresponding mechanical properties. Combining these results, it can be concluded that the primary tribo-corrosion mechanism of the TC4 is dominated by abrasion wear due to its lower hardness, resulting in the highest COF and the most active *OCP* (Fig. 3). The soft pristine TC4 results in a large extent of abrasive and adhesive wear, and generating a larger wear volume (Figs. 5 and 6). The pure mechanical wear effect causes the severe plastic deformation on the surface of TC4, resulting in the rough surface with high dislocation density, which directly accelerates the tribo-corrosion process [52,53].

The LSAed specimens exhibit higher tribo-corrosion resistance with lower COF, nobler *OCP* (Fig. 3) and lower wear volume (Fig. 5 and Table 6). It is well known that the hardness of materials plays a crucial role in their susceptibility to tribo-corrosion [54,55]. Acar and his co-workers found that the formation of TiO_2 on titanium surfaces not only increases surface hardness but also enhances tribo-corrosion resistance [54]. Owing to the increased hardness of the LSAed specimens, in accordance with Archard's law, the contact area between the Al_2O_3 ball and the surface of the specimen reduces, which contributes to the overall improvement in tribo-corrosion resistance [54,56]. In addition, the presence of Ti_2Cu in the Ti-based alloys improves resistance to plastic deformation, which in turn boosts wear resistance. Specifically, Ti—12Cu exhibits higher wear resistance compared to Ti-7.1Cu and Ti—3Cu due to this enhancement [10]. In the present study, the higher volume fraction of the hard intermetallic phases (Ti_2Cu and TiCu) in TC4-17Cu also helps to improve its tribo-corrosion resistance [18]. Ju and his co-workers have reported that the microstructure of the hyper-eutectoid TC4-Cu bulk alloys fabricated by LPBF consist of the nano Ti_2Cu phase which was detected using HRTEM [57]. The micro-hardness of the LPBFed TC4-Cu alloys gradually increases as the Cu content increases. The LPBFed TC4-10wt%Cu alloy is the hardest (596.8 HV) with the lowest wear rate owing to solid solution strengthening, fine-grain strengthening, and precipitation strengthening of the nano Ti_2Cu phase. In the present study, the hypereutectoid LSAed TC4-Cu coating with 17 *wt*% Cu also possesses the highest hardness and highest tribo-corrosion resistance due to the existence of more Ti—Cu intermetallic phases.

3.6. Mechanism of tribo-corrosion

The static corrosion mechanism of the TC4-Cu coatings in 0.9 wt% NaCl solution has been reported in [18]. The pristine TC4 possesses the highest corrosion resistance owing to the tenacious passive TiO_2 layer formed on the surface acting as a barrier against corrosion. For the LSAed specimen with a lower Cu content, i.e. TC4-6Cu, the micro-galvanic effect is less significant because the content of nobler Ti_2Cu (10.6 vol%) is much smaller than that of the more active α/β-Ti. Then the protective film still plays the role in inhibiting corrosion, resulting in higher the corrosion resistance as evidenced by lower I_{corr} (Table 5). For

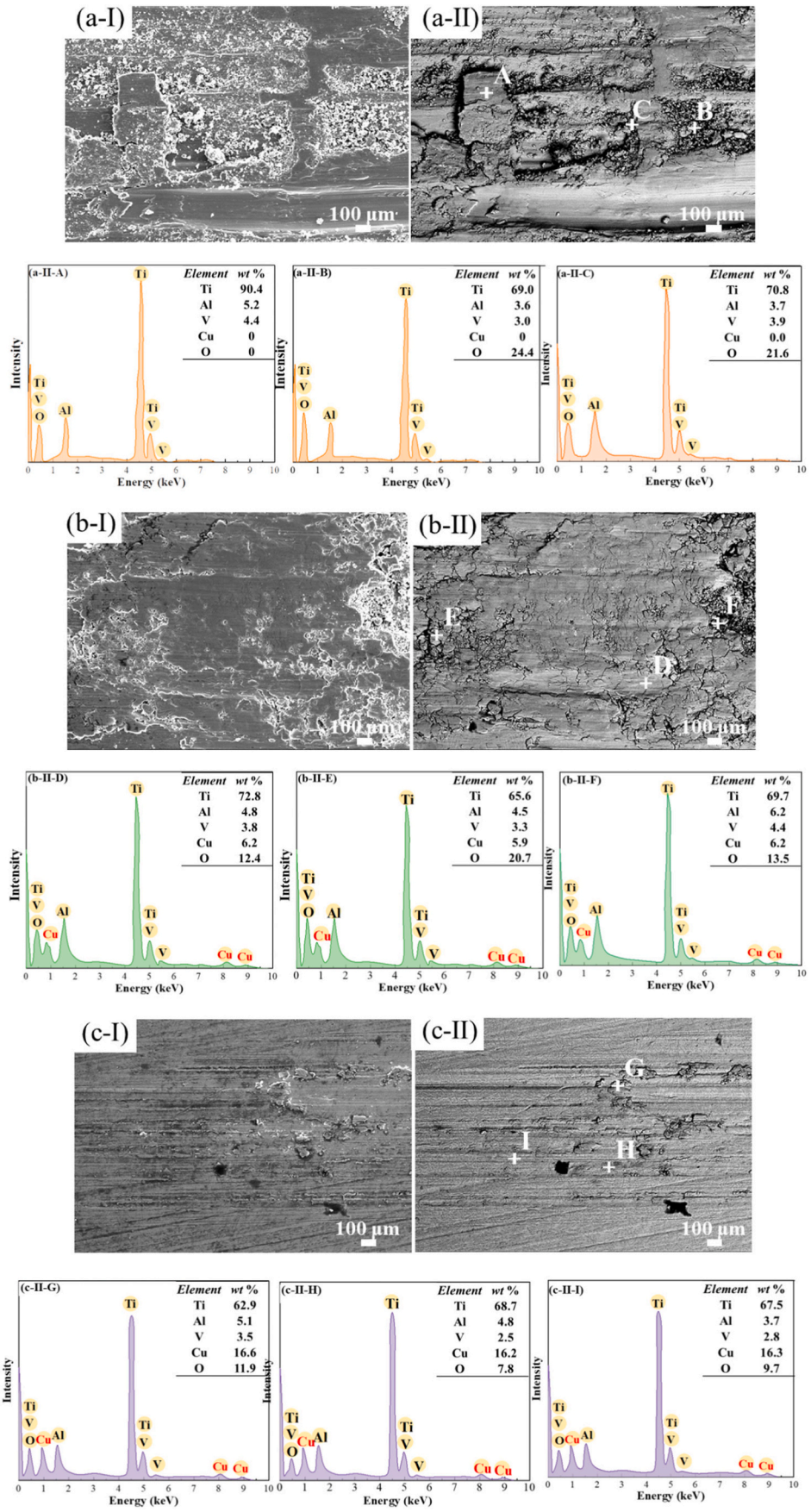

Fig. 6. SEM micrographs and EDS spectra of TC4 and LSAed specimens after tribo-corrosion test in 0.9 *wt*% NaCl solution at 37 °C: (a) pristine TC4, (b) TC4-6Cu and (c) TC4-17Cu. (I) and (II) correspond to the images taken by SE and BSE modes respectively.

Table 7
Components of wear and corrosion of various specimens.

Specimen	Components of wear, corrosion and synergism (mm/yr)								$a = \frac{\Delta C_w}{\Delta W_c}$ ($*10^{-3}$)
	T	C_0 ($*10^{-3}$)	C_W	$\triangle C_W$	W_0	S	$\triangle W_C$	W_C	
TC4	89.43	0.51	0.06	0.06	49.23	40.19	41.13	89.37	1.58
TC4-6Cu	70.00	0.55	0.05	0.04	37.37	32.63	32.58	69.96	1.35
TC4-17Cu	52.05	19.00	0.02	0.01	27.58	24.41	24.45	52.03	0.21

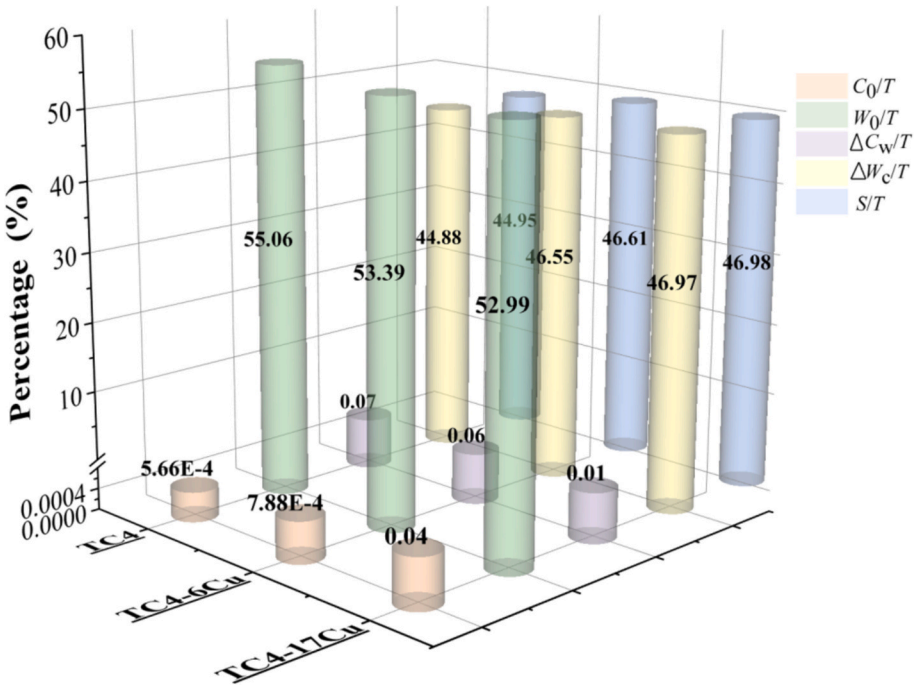

Fig. 7. Contributions of the components in tribo-corrosion for TC4 and LSAed TC4-Cu specimens in 0.9 *wt*% NaCl solution at 37 °C.

the LSAed specimens with a higher Cu content, i.e. TC4-17Cu, possesses a higher content of the nobler IMPs (Ti_2Cu and TiCu) (35.9 vol%) than that in TC4-6Cu leading to a more significant micro-galvanic effect and the higher I_{corr} (Table 5).

From Fig. 8, the passive film or material is removed as the Al_2O_3 ball successively slid against the specimens due to the huge difference in hardness between the pristine TC4 and the Al_2O_3 ball (Fig. 8a). Then, the pristine TC4 is in the active state and the NaCl solution migrated into the damaged sites and promoted material dissolution, resulting in more severe spalling and the material loss from the pristine TC4. The worn debris might adhere to the interface between the pristine TC4 and counter surface, which promotes the occurrence of abrasive wear (Fig. 6). Severe plastic deformation of the surface leads to the more material loss of the pristine TC4 (Table 6). On the other hand, the

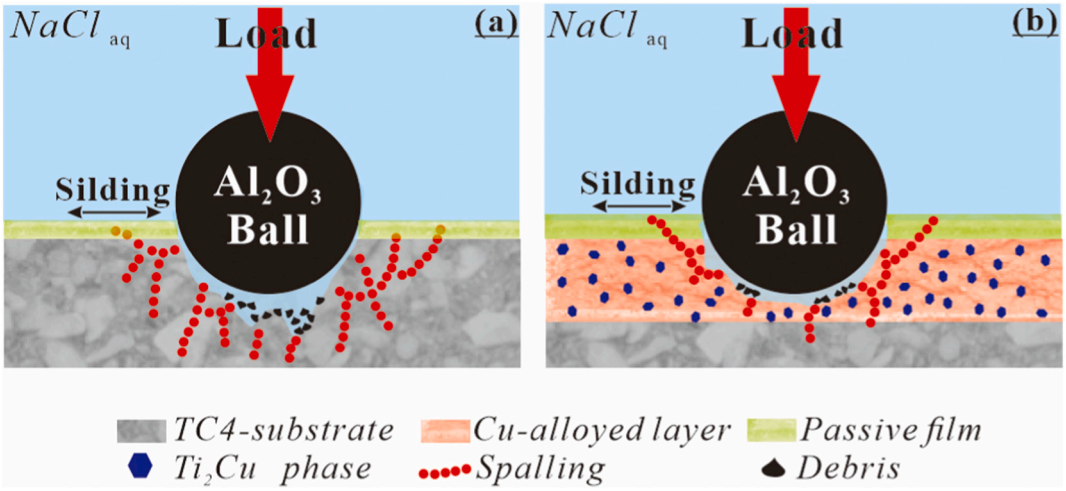

Fig. 8. Tribo-corrosion mechanisms of (a) pristine TC4 and (b) TC4-17Cu in 0.9 *wt*% NaCl solution.

galvanic couple formed between the undamaged region (cathode) and the worn track (anode) further promote corrosion of the specimens [58]. Stronger galvanic effect on the pristine TC4 is induced due to its more serious worn track (Fig. 6). It means that the abrasive wear and galvanic effect result in lower tribo-corrosion resistance of the pristine TC4. For the LSAed specimens, their higher hardness inhibits plastic deformation and delays the permeation of the NaCl solution, resulting in higher tribo-corrosion resistance. From Fig. 8b, TC4-17Cu with the highest hardness and the largest volume fraction of Ti_2Cu shows the least spalling, debris and the drastically lowest volume loss after the tribo-corrosion test. Meanwhile, galvanic corrosion is the least significant due to the smallest area of worn region. Both these factors lead to the highest tribo-corrosion resistance of TC4-17Cu.

4. Conclusions

The tribo-corrosion behavior of the LSAed TC4-Cu coatings with hypoeutectoid and hypereutectoid compositions (6 and 17 *wt*%) in 0.9 *wt*% NaCl solution at 37 °C is studied. The LSAed TC4-17Cu coating display higher tribo-corrosion resistance than that of the LSAed TC4-6Cu coating due to lower COF, higher hardness and nobler *OCP*, and the tribo-corrosion resistance of the pristine TC4 is the lowest. Based on the contributions of the different components, the tribo-corrosion of the coatings is found to be mainly attributed to mechanical wear, followed by wear-induced corrosion, while the electrochemical corrosion is negligible. The tribo-corrosion resistance of the LSAed TC4-Cu coatings is significantly improved because of the existence of the hard intermetallic phases (Ti_2Cu and TiCu), which effectively inhibit plastic deformation, reduce removal loss and galvanic effect between the worn and unworn regions during the tribo-corrosion process.

CRediT authorship contribution statement

Q. Qiao: Writing – original draft, Methodology, Investigation, Formal analysis, Data curation. **V.A.M. Cristino:** Validation, Investigation, Conceptualization. **L.M. Tam:** Project administration, Funding acquisition, Conceptualization. **C.T. Kwok:** Writing – review & editing, Supervision, Project administration, Investigation, Funding acquisition, Conceptualization.

Declaration of competing interest

The authors declare that they have no known competing financial interests or personal relationships that could have appeared to influence the work reported in this paper.

Acknowledgments

The present work was supported by the Science and Technology Development Fund (FDCT) of Macau SAR [File No. 0139/2020/A3] and the Institute for the Development and Quality, Macau.

Data availability

Data will be made available on request.

References

[1] M. Geetha, A. Singh, R. Asokamani, A. Gogia, Ti based biomaterials, the ultimate choice for orthopedic implants-a review, Prog. Mater. Sci. 54 (3) (2009) 397.
[2] M. Long, H.J. Rack, Titanium alloys in total joint replacement-a materials science perspective, Biomaterials 19 (18) (1998) 1621.
[3] M.A. Gepreel, M. Niinomi, Biocompatibility of Ti-alloys for long-term implantation, J. Mech. Behav. Biomed. Mater. 20 (2013) 407.
[4] F. Watari, A. Yokoyama, M. Omori, T. Hirai, H. Kondo, M. Uo, T. Kawasaki, Biocompatibility of materials and development to functionally graded implant for bio-medical application, Compos. Sci. Technol. 64 (6) (2004) 893.
[5] R. Banerjee, S. Das, K. Mukhopadhyay, S. Nag, A. Chakrabortty, K. Chaudhuri, Involvement of in vivo induced cheY-4 gene of Vibrio cholerae in motility, early adherence to intestinal epithelial cells and regulation of virulence factors, FEBS Lett. 532 (1–2) (2002) 221.
[6] T.M. Grupp, H.J. Meisel, J.A. Cotton, J. Schwiesau, B. Fritz, W. Blomer, V. Jansson, Alternative bearing materials for intervertebral disc arthroplasty, Biomaterials 31 (3) (2010) 523.
[7] E. Zhang, X. Zhao, J. Hu, R. Wang, S. Fu, G. Qin, Antibacterial metals and alloys for potential biomedical implants, Bioact 6 (8) (2021) 2569–2612.
[8] A.P. Zykova, A.V. Nikolaeva, A.V. Vorontsov, A.V. Chumaevskii, S.Y. Nikonov, E. N. Moskvichev, D.A. Gurianov, N.L. Savchenko, E.A. Kolubaev, S.Y. Tarasov, Phys. Mesomech. 262 (2023) 26.
[9] A. Zykova, A. Vorontsov, A. Nikolaeva, A. Chumaevskii, K. Kalashnikov, D. Gurianov, E. Kolubaev, Structural design and performance evaluation of Ti6Al4V/5% Cu produced by electron-beam additive technology with simultaneous double-wire feeding, Mater. Lett. 312 (2022) 131586.
[10] C. Peng, Y. Liu, H. Liu, S. Zhang, C. Bai, Y. Wan, K. Yang, Optimization of annealing treatment and comprehensive properties of Cu-containing Ti6Al4V-*x*Cu alloys, J. Mater. Sci. Technol. 35 (10) (2019) 2121–2131.
[11] E. Zhang, S. Li, J. Ren, L. Zhang, Y. Han, Effect of extrusion processing on the microstructure, mechanical properties, biocorrosion properties and antibacterial properties of Ti-Cu sintered alloys, Mater. Sci. Eng. C 69 (2016) 760–768.
[12] Z. Ma, L. Ren, R. Liu, K. Yang, Y. Zhang, Z. Liao, R.D.K. Misra, Effect of heat treatment on Cu distribution, antibacterial performance and cytotoxicity of Ti-6Al-4V-5Cu alloy, J. Mater. Sci. Technol. 31 (7) (2015) 723–732.
[13] R. Priya, C. Mallika, U.K. Mudali, Wear and tribocorrosion behaviour of 304L SS, Zr-702, Zircaloy-4 and Ti-grade2, Wear 310 (1) (2014) 90.
[14] S. Mischler, Sliding tribo-corrosion of passive metals: mechanisms and modeling, in: Third International Symposium on Tribo-Corrosion, ASTM International, 2013, pp. 1–18.
[15] A. Bronczyk, P. Kowalewski, M. Samoraj, Tribocorrosion behaviour of Ti6Al4V and AISI 316L in simulated normal and inflammatory conditions, Wear 434 (10) (2019).
[16] A.C. Alves, F. Oliveira, F. Wenger, P. Ponthiaux, J.P. Celis, L.A. Rocha, Tribocorrosion behaviour of anodic treated titanium surfaces intended for dental implants, J. Phys. D. Appl. Phys. 46 (40) (2013) 9.
[17] X. Huang, H. Liu, Z. Wang, L. Qiao, Y. Su, Y. Yan, Effect of surface oxidation on wear and tribocorrosion behavior of forged and selective laser melting-based TC4 alloys, Tribol. Int. 174 (2022) 107780.
[18] Q. Qiao, L.M. Tam, V.A.M. Cristino, C.T. Kwok, Surface hardness and corrosion behavior of laser surface-alloyed Ti6Al4V with copper, Surf. Coat. Technol. 444 (2022) 128663.
[19] ASTM Standard G133-22, Standard Test Method for Linearly Reciprocating Ball-on-flat Sliding Wear, ASTM International, West Conshohocken, PA, USA, 2022.
[20] ASTM Standard G119-09, Standard Guide for Determining Synergism Between Wear and Corrosion, ASTM International, West Conshohocken, PA, USA, 2021.
[21] Y. Sun, V. Rana, Tribocorrosion behaviour of AISI 304 stainless steel in 0.5 M NaCl solution, Mater. Chem. Phys. 129 (1–2) (2011) 138–147.
[22] K.C. Tekin, U. Malayoglu, Assessing the tribocorrosion performance of three different nickel-based superalloys, Tribol. Lett. 37 (3) (2010) 563–572.
[23] V. Guiñón Pina, V. Amigó, A. Igual Muñoz, Microstructural, electrochemical and tribo-electrochemical characterisation of titanium-copper biomedical alloys, Corros. Sci. 109 (2016) 115–125.
[24] ASTM Standard G102-89, Standard Practice for Calculation of Corrosion Rates and Related Information From Electrochemical Measurements, ASTM International, West Conshohocken, PA, USA, 2015.
[25] G.F. Sun, R. Zhou, Y.K. Zhang, G.D. Yuan, K. Wang, X.D. Ren, D.P. Wen, Microstructure evolution and lubricant wear performance of laser alloyed layers on automobile engine chains, Opt. Laser Technol. 62 (2014) 20–31.
[26] J. Li, B. Chen, M. Wang, C. Jing, Z. Fan, Z. Zhang, C. Zhang, Microstructure performance and nano-effect of laser alloying composites with multi-phase on TA1 titanium alloy, Opt. Laser Technol. 169 (2024) 109975.
[27] A. Myakinin, A. Turlybekuly, A. Pogrebnjak, A. Mirek, M. Bechelany, I. Liubchak, W. Simka, In vitro evaluation of electrochemically bioactivated Ti6Al4V 3D porous scaffolds, Mater. Sci. Eng. C 121 (2021) 111870.
[28] L. Bolzoni, F. Yang, X-ray diffraction for phase identification in Ti-based alloys: benefits and limitations, Phys. Scr. 99 (6) (2024) 065024.
[29] H. Donthula, B. Vishwanadh, T. Alam, Morphological evolution of transformation products and eutectoid transformation(s) in a hyper-eutectoid Ti-12 *at*% Cu alloy, Acta Mater. 168 (2019) 63–75.
[30] R. Dong, W. Zhu, C. Zhao, Y. Zhang, F. Ren, Microstructure, mechanical properties, and sliding wear behavior of spark plasma sintered Ti-Cu alloys, Metall. Mater. Trans. A 49 (12) (2018) 6147–6160.
[31] R.L. Li, J. Li, Y.N. Yan, M. Shao, Tribocorrosion resistance of CoCrFeNiNbx laser-clad coatings in the neutral and acid solutions, Opt. Laser Technol. 158 (2023) 108817.
[32] H. Liu, H. Liu, S. Zhang, H. Wang, X. Wei, L. Ren, K. Yang, Metastable pitting corrosion behavior of laser powder bed fusion produced Ti6Al4V-Cu in 3.5% NaCl solution, Corros. Sci. 223, 111452.
[33] Y. Zhang, X. Yin, J. Wang, F. Yan, Influence of microstructure evolution on tribocorrosion of S31254 steel in artificial seawater, Corros. Sci. 88 (2014) 423–433.
[34] P. Henry, J. Takadoum, P. Berçot, Depassivation of some metals by sliding friction, Corros. Sci. 53 (2011) 320–328.

[35] T. Yamamoto, K. Fushimi, M. Seo, S. Tsuri, T. Adachi, H. Habazaki, Depassivation re-passivation behavior of type-312L stainless steel in NaCl solution investigated by the micro-indentation, Corros. Sci. 51 (2009) 1545–1553.
[36] J. Chen, J. Wang, F. Yan, Q. Zhang, Q.A. Li, Effect of applied potential on the tribocorrosion behaviors of Monel K500 alloy in artificial seawater, Tribol. Int. 81 (2015) 1–8.
[37] M.P. Licausi, A.I. Muñoz, V.A. Borrás, Influence of the fabrication process and fluoride content on the tribocorrosion behaviour of Ti6Al4V biomedical alloy in artificial saliva, J. Mech. Behav. Biomed. 20 (2013) 137–148.
[38] B. He, C. Xin, Y. Chen, Y. Xu, Q. Zhao, Z. Hou, Y. Zhao, Biological performance and tribocorrosion behavior of in-situ synthesized Cu_xO/TiO_2 coatings, Appl. Surf. Sci. 600 (2022) 154096.
[39] M.P. Licausi, A.I. Muñoz, V.A. Borrás, Tribocorrosion mechanisms of Ti6Al4V biomedical alloys in artificial saliva with different pHs, J. Phys. D 46 (40) (2013) 404003.
[40] I. Toor, Repassivation kinetics and its role in SCC prediction-a review, Int. J. Electrochem. Sci. 9 (2014) 2737–2755.
[41] J. Lutz, S. Mändl, Reduced tribocorrosion of CoCr alloys in simulated body fluid after nitrogen insertion, Surf. Coat. Technol. 204 (18/19) (2010) 3043–3046.
[42] L. Xu, X. Fu, H. Su, H. Sun, R. Li, Y. Wan, Corrosion and tribocorrosion protection of AZ31B Mg alloy by a hydrothermally treated PEO/chitosan composite coating, Prog. Org. Coat. 170 (2022) 107002.
[43] K. Hu, X. Liu, S. Zhang, Z. Xue, Y. Yang, K. Yang, Tribocorrosion behavior of HVOF sprayed WC-based cermet coatings in sodium chloride solution environment in relation to binder phases, Surf. Coat. Technol. 435 (2022) 128248.
[44] M. Bao, X. Wang, L. Yang, G. Qin, E. Zhang, Tribocorrosion behavior of Ti-Cu alloy in hank's solution for biomedical application, J. Bio- and Tribo-Corros. 4 (2) (2018) 1–4.
[45] L. Cao, Y. Wan, S. Yang, J. Pu, The tribocorrosion and corrosion properties of thermally oxidized Ti6Al4V alloy in 0.9 *wt.*% NaCl physiological saline, Coatings 8 (8) (2018) 285.
[46] K.V. Smyrnova, A.D. Pogrebnjak, L.G. Kassenova, Structural features and properties of biocompatible Ti-based alloys with β-stabilizing elements, in: Advances in Thin Films, Nanostructured Materials, and Coatings: Selected Papers From the 2018 International Conference on "Nanomaterials: Applications & Properties", 2019, pp. 319–330.
[47] X. Lu, D. Zhang, W. Xu, A. Yu, J. Zhang, M. Tamaddon, B. Su, The effect of Cu content on corrosion, wear and tribocorrosion resistance of Ti-Mo-Cu alloy for load-bearing bone implants, Corros. Sci. 177 (2020) 109007.
[48] P. Lu, M. Wu, X. Liu, X. Miao, W. Duan, A tribocorrosion investigation of SLM fabricated ti6al4v nanocomposites by laser rescanning and GO mixing, Rapid Prototyp. J. 28 (2021) 32–40.
[49] J. Chavez, O. Jimenez, D. Bravo-Barcenas, L. Olmos, F. Alvarado-Hernandez, M. A. Gonzalez, M. Flores, Corrosion and tribocorrosion behavior of Ti6Al4V/*x*TiN composites for biomedical applications, T. Nonferr. Metal. Soc. 32 (2) (2022) 540–558.
[50] B. Zhang, J. Wang, J. Yuan, F. Yan, Tribocorrosion behavior of nickel-aluminium bronze sliding against alumina under the lubrication by seawater with different halide concentrations, Friction 7 (5) (2019) 444–456.
[51] M.M. Stack, G.H. Abdulrahman, Mapping erosion-corrosion of carbon steel in oil exploration conditions: some new approaches to characterizing mechanisms and synergies, Tribol. Int. 43 (7) (2010) 1268–1277.
[52] R. Namus, W.M. Rainforth, The influence of cathodic potentials on the surface oxide layer status and tribocorrosion behaviour of Ti6Al4V and CoCrMo alloys in simulated body fluid, Biotribology 30 (2022) 100212.
[53] Y. Si, H. Liu, H. Yu, X. Jiang, D.A. Sun, A heterogeneous $TiO_2/SrTiO_3$ coating on titanium alloy with excellent photocatalytic antibacterial, osteogenesis and tribocorrosion properties, Surf. Coat. Technol. 431 (2022) 128008.
[54] M.T. Acar, H. Kovacı, A. Çelik, Investigation of corrosion and tribocorrosion behavior of boron doped and graphene oxide doped TiO_2 nanotubes produced on Cp-Ti, Mater. Today Commun. 32 (2022) 104182.
[55] H. Wu, X. Zhang, X. He, M. Li, X. Huang, R. Hang, Wear and corrosion resistance of anti-bacterial Ti-Cu-N coatings on titanium implants, Appl. Surf. Sci. 317 (2014) 614–621.
[56] A.D. Pogrebnjak, M.A. Lisovenko, A. Turlybekuly, V.V. Buranich, Protective coatings with nanoscale multilayer architecture: current state and main trends, Phys-Usp+ 64 (3) (2021) 253.
[57] J. Jiang, Z. Rui, S. Zhao, W. Chenchen, P. Peng, W. Jun, S. Baode, X. Bo, L. Qian, Shaofei Liu, Tao Yang, Remarkable bioactivity, bio-tribological, antibacterial, and anti-corrosion properties in a Ti-6Al-4V-xCu alloy by laser powder bed fusion for superior biomedical implant applications, Chem. Eng. J. 471 (2023) 144656.
[58] Z. Wang, Y. Yan, L. Xing, Y. Su, L. Qiao, The role of hard phase carbides in tribocorrosion processes for a Co-based biomedical alloy, Tribol. Int. 113 (2017) 370–376.